JOURNAL OF MATERIALS SCIENCE 35 (2000) 4373–4378

Perovskite phase developments in $Pb[(Mg,Zn)_{1/3}Ta_{2/3}]O_3$ system and dielectric characteristics

SEUNG-MO LIM, NAM-KYOUNG KIM*
Department of Inorganic Materials Engineering Kyungpook National University
Taegu 702-701, Korea
E-mail: nkkim@knu.ac.kr

Stabilization of a perovskite structure was attempted by replacing Mg for Zn in $Pb(Zn_{1/3}Ta_{2/3})O_3$. System powders were prepared using a B-site precursor method by reacting PbO with separately-prepared precursor compositions. Effects of the substituent Mg concentration on perovskite phase developments and subsequent changes in dielectric properties were investigated, as a function of measurement frequency. Phase transition modes reflected in the dielectric constant spectra were analyzed in terms of diffuseness exponent and degree of diffuseness. Internal microstructures of the ceramics were examined, and correlations with perovskite phase contents and dielectric properties are discussed.

1. Introduction

Lead zinc niobate $Pb(Zn_{1/3}Nb_{2/3})O_3$ (PZN in short) is a disordered perovskite relaxor ferroelectric compound with diffuse phase transition (DPT) behaviors [1–3]. Perovskite PZN, however, can not easily be synthesized by conventional calcining-mixed-oxide processes at ambient pressure, but only under very high pressures [4], with the aids of fluxes [1, 3, 5–7], or very recently via mechanochemical reactions [8]. In contrast, it was reported that preparation of lead zinc tantalate $Pb(Zn_{1/3}Ta_{2/3})O_3$ (PZT; It should be remembered that PZT in this paper does not stand for $Pb(Zr,Ti)O_3$) in a perovskite structure is virtually impossible [9, 10], even by the methods used in perovskite PZN. It is interesting to note that perovskite PZN is synthesizable, while PZT is not, even though Nb and Ta possess the same ionic radii of 0.064 nm at 6-fold coordinations [11]. The reason behind such difficulties in the formation of perovskite PZT seems to be due, in part at least, to a smaller value of electronegativity difference [12] between tantalum and oxygen (as compared with that between niobium and oxygen), as the smaller difference would lead to more-covalent pyrochlore structures. Lead magnesium tantalate $Pb(Mg_{1/3}Ta_{2/3})O_3$ (PMT), a tantalum-analog of a prototype relaxor $Pb(Mg_{1/3}Nb_{2/3})O_3$ (PMN), is also a disordered perovskite ferroelectric relaxor [13–15]. Like PZN and PMN, PMT exhibits DPT behaviors [15–17]. It was also reported that PMT substitution to PZN by only 20 mol% partially stabilized (up to 40%) the perovskite structure [17].

So far, dielectric, crystallographic, and microstructural studies on PMT have been reported [13–20]. In contrast, little attention has been paid to PZT yet, due to extreme difficulties in stabilization to a perovskite structure. Nevertheless, it would be interesting to investigate the pseudobinary system PMT-PZT, as perovskite structure developments in PZT (by solid-state reactions at atmospheric pressure) is expected to be promoted by PMT substitution. Besides, the low dielectric maximum temperature of PMT is also expected to be increased by the influence of PZT, considering gradual increases in the dielectric maximum temperatures with composition change from PMN to PZN [21]. In the present study, therefore, perovskite structure stabilization in $Pb(Zn_{1/3}Ta_{2/3})O_3$ by substitution of Zn by isovalent but smaller-sized (0.074 versus 0.072 nm [11]) and more oxygen-affinite [12] Mg ions was attempted. The greater electronegativity difference between magnesium and oxygen would help favoring for an ionic-bonded perovskite structure.

Syntheses of monophasic perovskite in $Pb(B^{2+}{}_{1/3}B''_{2/3})O_3$ ($B'' = Nb$ or Ta) by traditional solid-state reactions are known to be greatly interfered by parasitic pyrochlore phase(s) of $PbO\text{-}(B^{2+}O)\text{-}(Nb/Ta)_2O_5$ composition. In order to increase the perovskite phase yields by suppressing the formations of such pyrochlore(s), a B-site precursor method [22, 23] (most well-known of which is the columbite process [24]) was adopted in the present study. The process in the present PMT-PZT system, therefore, involves prereactions of MgO, ZnO, and Ta_2O_5 to form B-site

* Author to whom all correspondence should be addressed.

precursor compositions of $(B'_{1/3}B''_{2/3})O_2$-type prior to reactions with PbO.

2. Experimental

The system under investigation is $Pb[(Mg_yZn_{1-y})_{1/3}Ta_{2/3}]O_3$ (i.e., yPb$(Mg_{1/3}Ta_{2/3})O_3$-$(1-y)$Pb$(Zn_{1/3}Ta_{2/3})O_3$ or yPMT-$(1-y)$PZT), with values of y ranging from 0.0 to 1.0 at regular steps of 0.2. Commercial oxide powders of PbO (purity $\geq$99.5%), MgO (99.9%), ZnO (99.8%), and Ta_2O_5 (99.9%) were used as starting materials. In order to maintain stoichiometries as closely to the nominal compositions as possible, moisture contents of raw chemicals and synthesized precursor powders were measured and introduced to the batch calculations.

Required amounts of B-site forming chemicals were weighed, wet-milled under alcohol (using ZrO_2 ball in a polyethylene bottle), dried overnight, and calcined at 1100–1250°C for 2 h to form precursor oxide system of yMgTa$_2$O$_6$-$(1-y)$ZnTa$_2$O$_6$. Prepared powders were reacted with PbO for 2 h at 800–1000°C, also in stoichiometric proportions (i.e., without any addition of excess PbO), to form yPMT-$(1-y)$PZT (or PMZT in short) system compositions. During the syntheses of B-site precursors and PMZT system powders, calcination processes were repeated once, with introduction of additional milling and drying steps, to assist the phase formations, which were examined by powder X-ray diffraction (XRD). Perovskite phase contents were calculated by comparing intensity maxima of major diffraction peaks, $I_{\text{perov}(110)}/(I_{\text{perov}(110)} + I_{\text{pyro}(222)})$.

Pellet-type samples (10 mm in diameter and ~1 mm thickness) were uniaxially pressed using the PMZT system powders (added with polyvinyl alcohol binder of 2 wt% dilute solution for ready dispersion) and were further compacted isostatically at 100 MPa. To suppress lead loss at high temperatures, the pellets were embedded in atmosphere powders of identical composition and were fired in a double-enclosure setup (with $PbZrO_3$ powder used as crucible sealant [17]) at 1150–1300°C for 1 h, after 1 h hold at 600°C for binder burn-out. Optimum sintering conditions were determined by considering the perovskite phase yields and fired densities. Bulk densities were evaluated using geometrical dimensions, after grinding and polishing to make the surfaces parallel. Major faces of the pellets were covered with sputtered gold as electrodes. Weak-field (~1.0 V_{rms}/mm) radio-frequency (1, 10, 100, and 1000 kHz) dielectric constants and losses of the system ceramics were measured using a computer-interfaced impedance analyzer over −175–230°C on cooling. Hysteresis responses were monitored using a ferroelectric test system. Microstructures of the fractured specimens were examined by scanning electron microscopy.

3. Results and discussion

XRD spectra of the B-site precursor system powders are shown in Fig. 1a. Whereas a tri-αPbO_2 structure ($ZnTa_2O_6$: JCPDS #39-1484) was observed at up to $y = 0.4$, trirutile ($MgTa_2O_6$: JCPDS #32-631) was detected down to $y = 0.2$. Hence, mixed phases of the

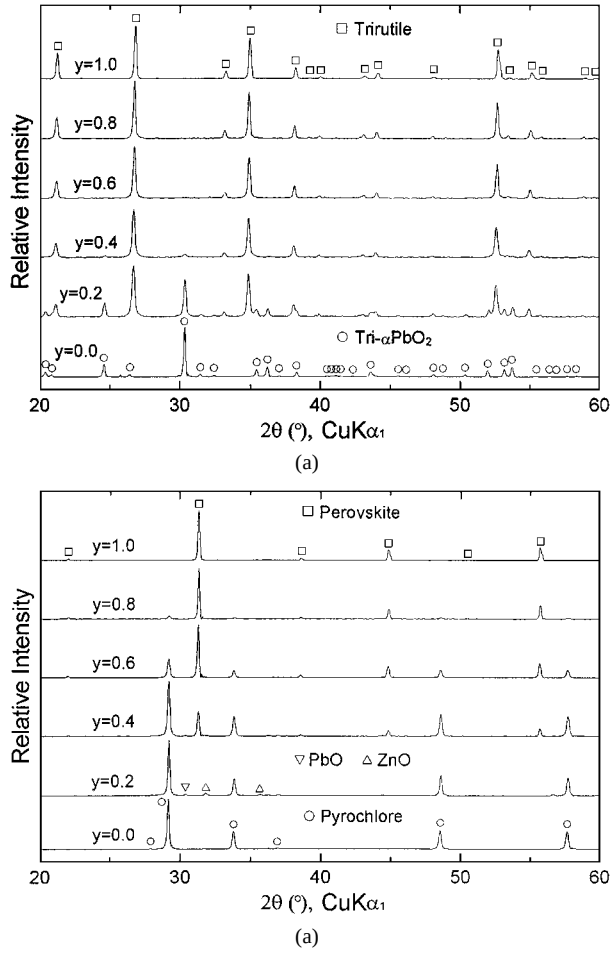

Figure 1 X-ray diffraction patterns of (a) B-site precursor yMgTa$_2$O$_6$-$(1-y)$ZnTa$_2$O$_6$ and (b) yPMT-$(1-y)$PZT systems (after second calcination).

two structures coexisted at intermediate compositions of $y = 0.2$ and 0.4, implying limited solubility in the B-site precursor system. The limited solubility is due probably to dissimilar structures of the end components. On the other hand, only tri-αPbO_2 or trirutile existed at $y = 0.0$ or at $0.6 \leq y \leq 1.0$, respectively, indicating that the trirutile structure has a wider composition range of solid solubility. Meanwhile, very small shifts in diffraction angles of the trirutile to lower values with decreasing y (i.e., Mg concentration) were detected, which can be explained by gradual replacement of Mg by Zn of larger ionic size: 0.072 versus 0.074 nm [11].

In Fig. 1b are the phase development results in the PMZT system. Even by the B-site precursor method, no trace of a perovskite structure was detected at $y = 0.0$ of stoichiometric PZT composition. Instead, only pyrochlore, with negligible amounts of PbO and ZnO, existed. The two oxides could possibly be the leftover components after the formation of cubic pyrochlore $Pb_{1.83}(Zn_{0.29}Ta_{1.71})O_{6.39}$ (JCPDS #34-395) from stoichiometric mixtures of PbO : ZnO : $Ta_2O_5 = 3:1:1$ by mol (intended for perovskite development). The situation was not improved even after replacement by 20 mol% Mg ($y = 0.2$). With further substitutions by Mg, then, a perovskite structure started to develop at $y = 0.4$, but the pyrochlore was still the major phase. At $y = 0.6$ and 0.8, intensities of the perovskite increased

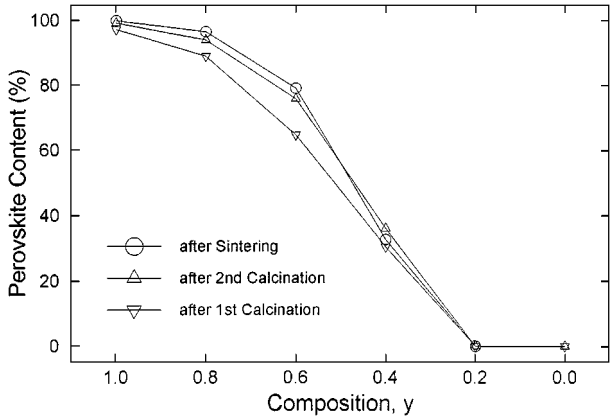

Figure 2 Perovskite phase yields after calcinations and sintering.

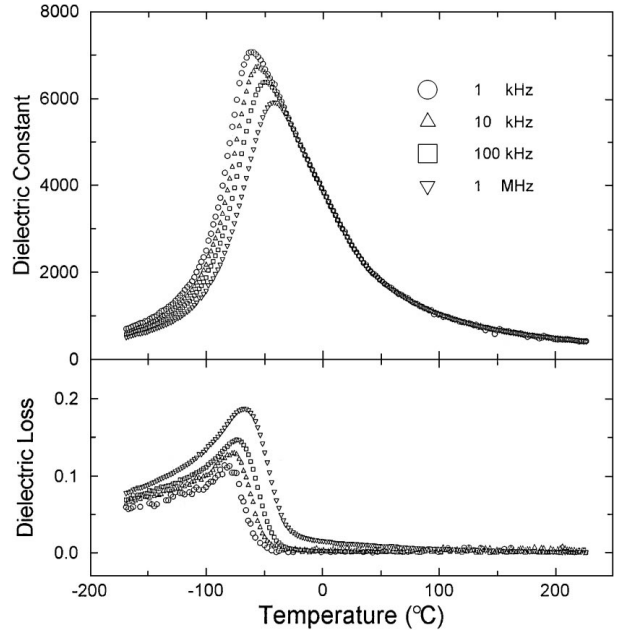

Figure 3 Dielectric constant and loss spectra of $y = 0.8$ at different frequencies.

at the expense of pyrochlore (along with leftover PbO and ZnO). Finally at $y = 1.0$ of stoichiometric PMT composition, only a well-developed perovskite structure was observed. Meanwhile, no superlattice reflections were detected at intermediate compositions, implying lack of any macroscopic ordering among the B-site octahedral species, similar to the disordered states at the end components.

Perovskite phase yields of the system powders (after first and second calcinations, and after sintering) are plotted in Fig. 2. The contents after sintering were estimated using the atmosphere powders. At $y = 0.0$ (i.e., PZT), however, sintering was not accomplished properly due to the appearance of liquid phase, so the perovskite content after sintering could not be included. It should be noticed that the abscissa is drawn in a descending scale in order to conform to the idea that the composition with a lower dielectric maximum temperature be located at lefthand side of the composition axis. As was discussed in Fig. 1b, the perovskite contents were 0% at $y \leq 0.2$. The contents increased rapidly to 33% (after sintering) at $y = 0.4$, increased further with more substitutions by Mg, and finally became saturated at $y = 1.0$. Therefore, threshold Mg concentration of perovskite structure development seems to lie at $0.2 < y < 0.4$. Meanwhile, for a given composition above the threshold concentration, the perovskite content increased somewhat after sintering, as compared with the values after first and second calcinations. At $y = 0.4$, however, the content decreased after the second calcination (36% → 33%). The decrease seems to be resulted from the lead loss, occurred preferentially at Mg-poor compositions (i.e., low values of y), where pyrochlore formations would have produced leftover PbO. Similar cases were also observed at other pyrochlore-rich compositions in a PMT-PZT-PZN system [25]. Meanwhile, it was reported that only 40 mol% PMN substitution was sufficient to stabilize the perovskite structure (up to >98%) in PZN [21], whereas perovskite content of 72% was resulted by the same amount of PMT substitution [17], implying that lead-based tantalate composition is more refractory in the perovskite stabilization. Besides, by comparison with the present results, it can be deduced that Mg substitution is less effective in tantalate system, as in the niobate system. It can also be concluded that PZN is more easily stabilized than PZT, which supports the inability of the synthesis of perovskite PZT yet.

Fig. 3 shows frequency-dependent dielectric constant and loss spectra of representative composition $y = 0.8$ (0.8PMT–0.2PZT), where the perovskite phase content was 97% (after sintering). Maximum dielectric constants and dielectric maximum temperatures were 7,100 (−62°C), 6,700 (−57°C), 6,400 (−50°C), and 5,900 (−42°C) at 1, 10, 100, and 1000 kHz, respectively. Meanwhile, magnitudes of the maximum losses were ∼11% (∼−79°C), 13% (−77°C), 15% (−74°C), and 19% (−68°C) at the same frequency decades. Hence, the dielectric spectra showed typical relaxor behaviors of gradually decreasing maximum dielectric constants and increasing dielectric maximum temperatures (together with increasing maximum dielectric losses and corresponding temperatures), as the measurement frequency increased. Peak temperatures of the loss spectra were somewhat lower (by 17–26°C) than those of the dielectric constants, which is usual in relaxor ferroelectric compositions. Similar dielectric relaxations were observed at other compositions as well, except for $y = 0.2$.

Dielectric constant spectra (@ 1 kHz) of the system ceramics are compared in Fig. 4. At the composition of $y = 0.2$ (0.2PMT–0.8PZT; perovskite content = 0%), only ever-decreasing values were observed, with room temperature dielectric constant and temperature coefficient of approximately 75 and −0.035/K, regardless of frequency. In contrast, the dielectric spectra of $0.4 \leq y$ showed dielectric maximum peaks with DPT behaviors. With increasing Mg substitutions, the maximum dielectric constant increased steeply, whereas the dielectric maximum temperatures decreased rather slowly.

Composition- and frequency-dependent maximum dielectric constants (K_{max}) and dielectric maximum temperatures (T_{max}) are replotted in Fig. 5, where those of $y = 0.2$ could not be included due to unavailability of corresponding data (Fig. 4). A very low maximum

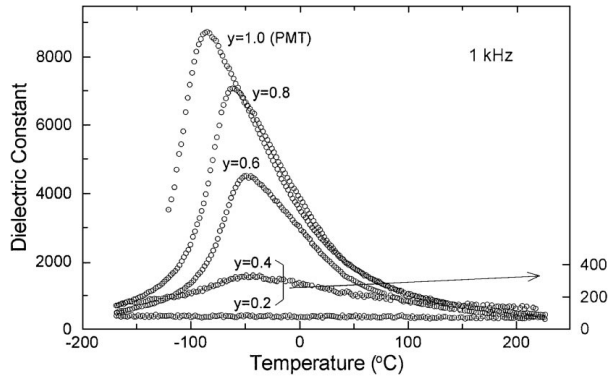

Figure 4 Dielectric constant spectra of the PMZT system ceramics.

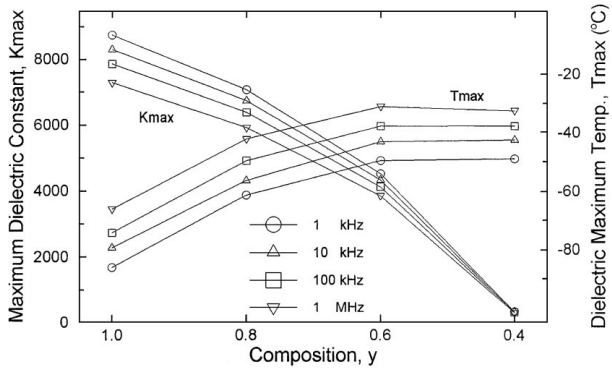

Figure 5 Dependences of maximum dielectric constants and dielectric maximum temperatures upon measurement frequency and composition.

dielectric constant value of ~330 (@ 1 kHz) at the composition of $y = 0.4$ (just above the threshold Mg concentration), where perovskite content was 33% after sintering, increased rapidly to 8,700 at $y = 1.0$. On the other hand, a dielectric maximum temperature of -49°C (@ 1 kHz) at $y = 0.4$ decreased continuously to -50°C ($y = 0.6$), -62°C ($y = 0.8$), and -86°C ($y = 1.0$). From the dielectric maximum temperatures in the composition range of $0.4 \leq y \leq 1.0$, that of perovskite PZT (i.e., $y = 0.0$) could be extrapolated to be -50–-40°C. Meanwhile, $\Delta T_{\max}(=T_{\max,1\,\mathrm{MHz}} - T_{\max,1\,\mathrm{kHz}})$ were 16, 18, 19, and 20°C at $y = 0.4$, 0.6, 0.8, and 1.0, respectively, which are quite insensitive to the composition change throughout the whole system. Likewise, $K_{\max}$ ratios ($=K_{\max,1\,\mathrm{MHz}}/K_{\max,1\,\mathrm{kHz}}$) were actually 92, 85, 84, and 83% for the same compositions, which are also rather insensitive to the composition change, even though the absolute values of difference between 1 kHz and 1 MHz increased substantially with increasing y.

Dielectric constant spectra in the paraelectric temperature range are widely described by an empirical power form [26, 27] as

$$\frac{1}{K} = \frac{1}{K_{\max}} + \frac{(T - T_{\max})^{\gamma}}{C},$$

where γ is a diffuseness exponent, varying between 1 and 2 for typical (first-order) sharp and (second-order) diffuse phase transitions. The values of γ can be obtained from gradients in the plot of $\log(1/K - 1/K_{\max})$ versus $\log(T - T_{\max})$, Fig. 6a ($y = 0.8$). Such-obtained

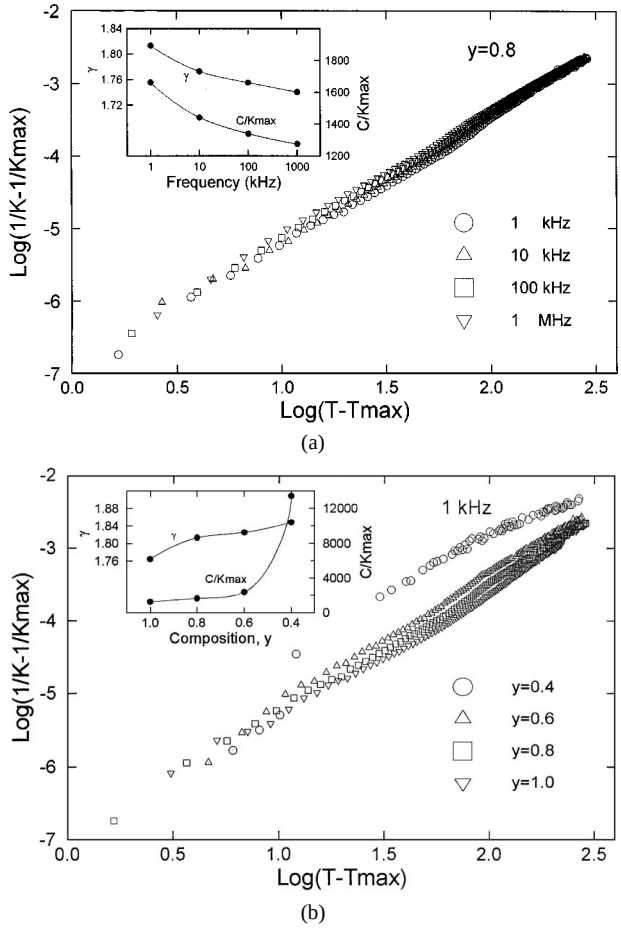

Figure 6 $\mathrm{Log}(1/K - 1/K_{\max})$ versus $\log(T - T_{\max})$, as functions of (a) measurement frequency at $y = 0.8$ and (b) composition at 1 kHz. In the insets are shown the variations of diffuseness exponent (γ) and degree of diffuseness ($C/K_{\max}$).

γ are separately plotted in the inset. The slight decrease in the values of γ with increasing frequency implies that the phase transition modes at lower frequencies are more close to diffuse ones. Also plotted in the inset are relative degrees of diffuseness, $C/K_{\max}$ [28], which were estimated from the values of C (read from intercepts in Fig. 6a at $\log(T - T_{\max}) = 0$) divided by corresponding values of $K_{\max}$. The four data sets in the plot, however, are so closely spaced that they could not easily be resolved, hence giving only slight differences in the values of γ and subsequent $C/K_{\max}$. Similar plots for examination of composition dependence are

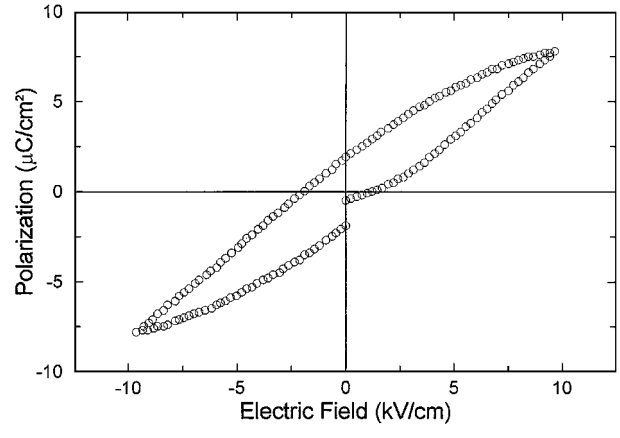

Figure 7 Ferroelectric hysteresis loop of $y = 0.8$ at -103°C.

presented in Fig. 6b. With increasing y, the values of γ and C/K_{max} decreased in general, indicating comparatively sharper dielectric spectra at higher Mg concentrations. C/K_{max} of $y = 0.4$, however, was much higher than those of the other three compositions, which is mainly due to the very small value of K_{max} (Fig. 5). Nevertheless, the values of γ changed only slightly, similar to the variations with frequency change (Fig. 6a inset).

In Fig. 7 is displayed a P-E hysteresis loop of $y = 0.8$ monitored at -103°C (well below the phase transition temperature of -62°C at 1 kHz), where a ferroelectric character is well demonstrated. Remnant polarization and coercive field were 1.9 μC/cm^2 and 1.9 kV/cm, respectively. Gradual disappearance of the hysteretic nature with increasing temperatures (up to the phase transition temperature) was observed. In the paraelectric temperature range, in contrast, linear relationships between polarization and electric field were maintained with the gradients steadily decreasing, due to reduction in the dielectric constant values.

Fracture micrographs of the system ceramics are contrasted in Fig. 8. Only submicrometer-sized grains of pyrochlore were present at a PZT-rich composition of $y = 0.2$, whereas larger perovskite grains crystallized locally in the pyrochlore matrix at $y = 0.4$. With further increase in Mg concentration, perovskite grains increased in volume ratio and became predominant at $0.8 \leq y$ at the expense of pyrochlore. Finally at $y = 1.0$ (PMT), only multi-faceted perovskite grains (up to $\sim$10 μm in size) were observed. The microstructure examinations were in consistent with the perovskite phase content data (Fig. 2), verifying the threshold Mg concentration of $0.2 < y < 0.4$. Variations in the dielectric constant data (Fig. 5) are also in consistent, in that the larger the portions of the perovskite phase (i.e., the higher the Mg concentration), the higher the maximum dielectric constants.

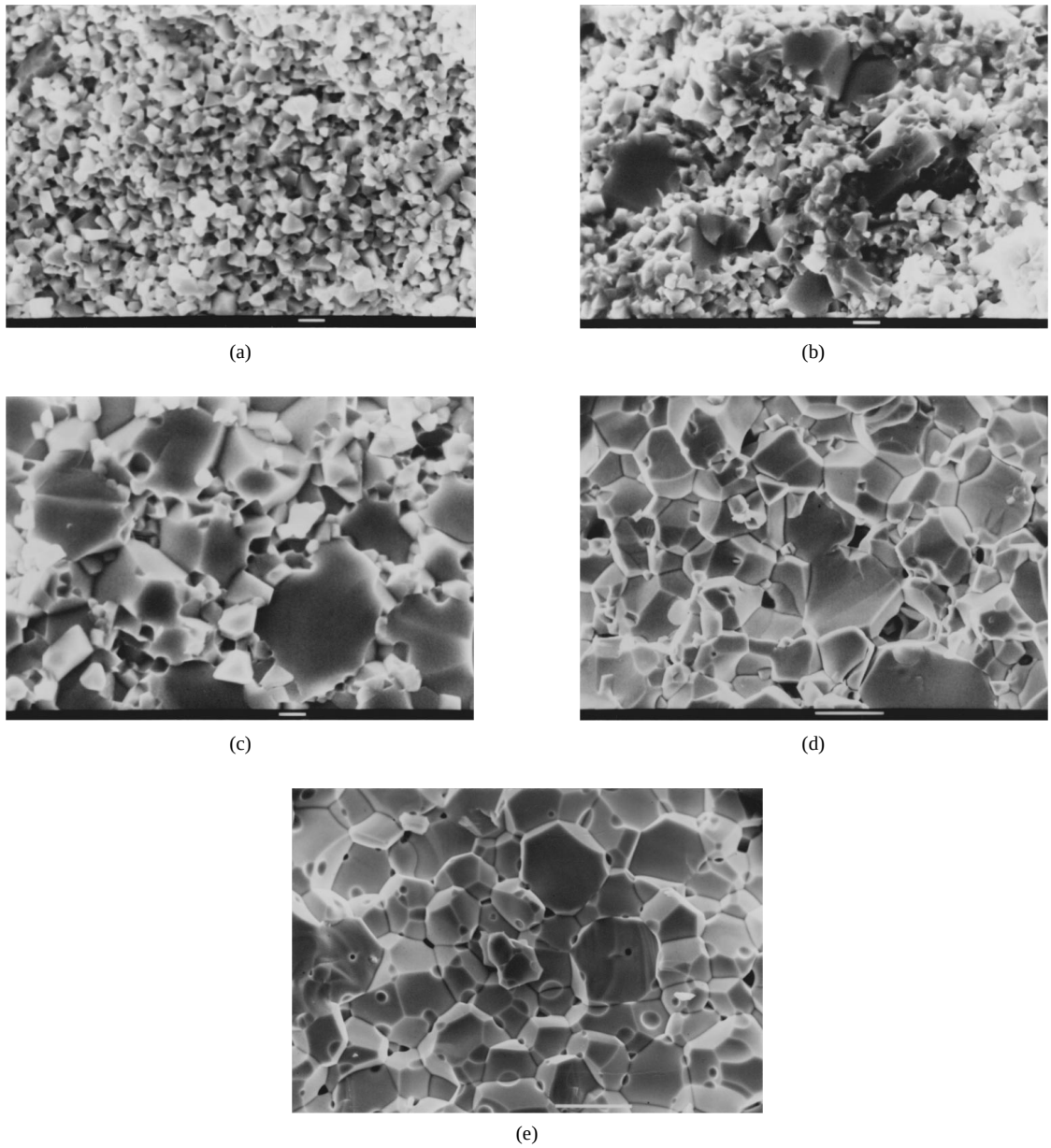

Figure 8 Microstructures of the system ceramics of (a) $y = 0.2$, (b) $y = 0.4$, (c) $y = 0.6$, (d) $y = 0.8$, and (e) $y = 1.0$ (PMT). scale bar = 1 μm (a)–(c) and 10 μm (d) and (e).

4. Summary

In the B-site precursor system, diphasic mixtures were observed at intermediate compositions of $y = 0.2$ and 0.4, implying limited solubility between the end components of $MgTa_2O_6$ (trirutile structure) and $ZnTa_2O_6$ (tri-αPbO_2 structure). In the PMZT system, only a pyrochlore structure was detected at $y \leq 0.2$. With increase in Mg concentration, a perovskite structure started to develop at $y = 0.4$, increased in contents, and finally became the sole phase at $y = 1.0$ (PMT). Typical dielectric relaxation with DPT behaviors were observed at $0.4 \leq y$. As the composition changed from $y = 0.4$ to $y = 1.0$, a very low maximum dielectric constant of $\sim$330 increased rapidly to 8,700, whereas a dielectric maximum temperature of $-49^{\circ}C$ decreased continuously to $-86^{\circ}C$ (@1 kHz). Meanwhile, diffuseness exponent and degree of diffuseness at a fixed composition of $y = 0.8$ decreased gently with increasing frequency. On the other hand, the former parameter decreased only slightly, whilst the latter decreased rapidly then slowly, with increasing substituent Mg concentration, indicating more broadness at Mg-poorer compositions. Ferroelectric hysteresis loops were observed at temperatures below the phase transition. Phase constitutions from the fracture micrographs showed good consistency with the results of perovskite phase contents and dielectric constant spectra.

Acknowledgements

This study was supported by the Korea Research Foundation under contract #1997-001-E00643.

References

1. V. A. BOKOV and I. E. MYL'NIKOVA, *Sov. Phys.-Solid State* **2** (1961) 2428.
2. S. NOMURA, T. TAKAHASHI and Y. YOKOMIZO, *J. Phys. Soc. Jpn.* **27** (1969) 262.
3. Y. YOKOMIZO, T. TAKAHASHI and S. NOMURA, *ibid.* **28** (1970) 1278.
4. Y. MATSUO, H. SASAKI, S. HAYAKAWA, F. KANAMARU and M. KOIZUMI, *J. Am. Ceram. Soc.* **52** (1969) 516.
5. Y. YOKOMIZO and S. NOMURA, *J. Phys. Soc. Jpn.* **28**(Suppl.) (1970) 150.
6. S.-E. PARK, M. L. MULVIHILL, P. D. LOPATH, M. ZIPARRO and T. R. SHROUT, in Proc. 10th IEEE ISAF, 1996, p. 79.
7. C. S. PARK, K. Y. LIM, D. Y. CHOI and S. J. CHUNG, *J. Kor. Phys. Soc.* **32**(Suppl.) (1998) S974.
8. J. WANG, D. WAN, J. XUE and W. B. NG, *J. Am. Ceram. Soc.* **82** (1999) 477.
9. T. R. SHROUT and A. HALLIYAL, *Am. Ceram. Soc. Bull.* **66** (1987) 704.
10. H. C. LING, M. F. YAN and W. W. RHODES, *Ferroelectrics* **89** (1989) 69.
11. R. D. SHANNON, *Acta Cryst.* **A32** (1976) 751.
12. W. F. SMITH, in "Principles of Materials Science and Engineering" 2nd ed. (McGraw-Hill, Singapore, 1990) p. 37.
13. K. UCHINO and S. NOMURA, *J. Phys. Soc. Jpn.* **41** (1976) 542.
14. N. SETTER and I. LAULICHT, *Appl. Spectrosc.* **41** (1987) 526.
15. B. A. MALKOV and YU. N. VENEVTSEV, *Inorg. Mater.* **13** (1977) 1189.
16. M.-C. CHAE and N.-K. KIM, *Ferroelectrics* **209** (1998) 603.
17. M.-C. CHAE, N.-K. KIM, J.-J. KIM and S.-H. CHO, *ibid.* **211** (1998) 25.
18. Z. G. LU, C. FLICOTEAUX and G. CALVARIN, *Mater. Res. Bull.* **31** (1996) 445.
19. M. A. AKBAS and P. K. DAVIES, *J. Mater. Res.* **12** (1997) 2617.
20. *Idem., J. Am. Ceram. Soc.* **80** (1997) 2933.
21. M.-C. CHAE, N.-K. KIM, J.-J. KIM and S.-H. CHO, *J. Mater. Sci.* **33** (1998) 1343.
22. B.-H. LEE, N.-K. KIM, J.-J. KIM and S.-H. CHO, Ferroelectrics **211** (1998) 233.
23. B.-H. LEE, N.-K. KIM and B.-O. PARK, *Ferroelectrics* **227** (1999) 87.
24. S. L. SWARTZ and T. R. SHROUT, *Mater. Res. Bull.* **17** (1982) 1245.
25. N.-K. KIM, unpblished data.
26. K. UCHINO and S. NOMURA, *Ferroelectrics Lett.* **44** (1982) 55.
27. M. KUWABARA, S. TAKAHASHI, K. GODA, K. OSHIMA and K. WATANABE, *Jpn. J. Appl. Phys.* **31** (1992) 3241.
28. S. J. BUTCHER and N. W. THOMAS, *J. Phys. Chem. Solids* **52** (1991) 595.

Received 30 June 1999
and accepted 16 February 2000